Journal Name

ARTICLE

Luminescent Solar Concentrators: Boosted Optical Efficiency by Polymer Dielectric Mirrors

Received 00th January 20xx,
Accepted 00th January 20xx

DOI: 10.1039/x0xx00000x

www.rsc.org/

G. Iasilli,[a] R. Francischello,[a] P. Lova,[b] S. Silvano,[b] A. Surace,[b] G. Pesce,[b] M. Alloisio,[b] M. Patrini,[c] M. Shimizu,[d] D. Comoretto,[b]* A. Pucci,[a]*

We report on the optical efficiency enhancement of luminescent solar concentrators based on a push-pull fluorophore realized using high dielectric contrast polymer distributed Bragg reflectors as back mirrors. The Bragg stacks are obtained alternating layers of cellulose acetate to thin films of a new stable and solution processable hydrated titania-poly(vinyl alcohol) nanocomposite (HyTiPVA) with refractive index higher than 1.9 over a broad spectral range. The results gathered with these systems are compared with enhancements provided by standard Bragg reflectors made of commercial polymers. We demonstrate that the application of the Bragg stacks with photonic band-gap tuned to the low energy side of the dye emission spectrum induces a 10% enhancement of optical efficiency. This enhancement is the result of a performing photon recycling mechanism and is retained even on a scaled-up device where the Bragg mirrors are used in a mosaic configuration.

Introduction

Nowadays, cost reduction and efficiency enhancement are the driving forces for technological development of photovoltaic (PV) systems.[1] In recent years, luminescent solar concentrators (LSCs) became appealing thanks to light weight, high concentration factors, and to the possibility to operate with diffuse light without the need of expensive solar trackers and coolers.[2] Moreover, these devices can be easily integrated into modern buildings, also accordingly to the EU guideline 2010/31/UE, which will require each new building to be almost zero energy consumption starting from 2020.

Even though LSCs are already available on the market,[3] some drawbacks are still limiting their massive commercial distribution. Such drawbacks include difficulties in the preparation of easily mountable modules and in the improvement of the device efficiency, which can be understood analyzing the LSC working principle. LSCs are highly transparent, planar and relatively thick waveguides doped with high quantum yield fluorophores.[2] The slabs have refractive index larger than the surrounding. In this way they favor total internal reflection of light emitted within the slab and its guiding to its sides, where standard solar cells are placed.[2] Notwithstanding their simplicity, several processes rule and limit their global device efficiency (η_{dev}), including the usually poor matching between the fluorophore absorption spectrum and the solar emission (η_{ABS}) as well as the dye emission efficiency (η_{PL}). Beside the issues related to the fluorophore, the efficiency of the lateral solar cells (η_{PV}), of the waveguiding (η_{WG}), and of the trapping processes (η_{trap}) affect the entire energy generation process such that:

$$\eta_{dev} = \eta_{ABS}\,\eta_{PL}\eta_{WG}\,\eta_{PV}\,\eta_{trap} \quad (1)$$

Concerning η_{abs}, several researchers focused on the development of new fluorophores with large spectral absorption and on tuning such absorption in the near infrared part of the solar spectrum, while maintaining the device transparency.[2, 4-6] To this end, high efficiency quantum dots synthesized without commonly used toxic heavy metals are very promising.[4] Conversely, if colored LSCs are chosen for aesthetic purposes, the efficiency can be increased by using smart near-infrared scatterers to funnel the non-absorbed long-wavelength solar radiation into the waveguide.[7, 8] Regarding η_{PL}, several dyes with quantum yield close to unity have been proposed.[2] On the other hand, self-absorption effects hinder η_{PL}, especially when large area devices and high fluorophore concentration are used. This drawback has been widely addressed engineering the fluorophore to maximize the Stokes shift. Moreover, Förster energy transfer has been investigated for molecular fluorophores, but the need to achieve proper blending on large area makes their use challenging.[2] To this end, donor-acceptor core-shell quantum dots are instead promising thanks to the possibility to couple different materials and achieve large Stokes shifts by simple wet chemistry.[4, 9, 10] The use of fluorogenic dye exploiting molecular aggregation or push-pull molecules could be an alternative approach to the problem.[11-14] Then, while molecular aspects, photoluminescence, and device efficiencies have been widely

[a] Dipartimento di Chimica e Chimica Industriale, Università di Pisa, via Moruzzi 13, 56124 Pisa, Italy. E-mail: davide.comoretto@unige.it
[b] Dipartimento di Chimica e Chimica Industriale, Università di Genova, Via Dodecaneso 31, 16146 Genova, Italy. E-mail: andrea.pucci@unipi.it
[c] Dipartimento di Fisica, Università di Pavia, via Bassi 6, 27100 Pavia, Italy
[d] Faculty of Molecular Chemistry and Engineering, Kyoto Institute of Technology, 606-8585 Kyoto, Japan

† Electronic Supplementary Information (ESI) available: [Additional information reported are: hybrid titania-PVA Nanocomposite Optical Constants (S1); Diffuser and LSC Characterization (S2); Optical characterization of the DBRs (S3); Optical Efficiency Measurement Details (S4).]. See DOI: 10.1039/x0xx00000x

Please do not adjust margins

addressed and understood,[2, 15, 16] many strategies are still under investigation for the enhancement of η_{trap}.[17] In this work, we propose a new approach to enhance such parameter, while leaving the other efficiencies unchanged. For a waveguide with refractive index n_{slab}~1.5 η_{trap} is evaluated as:

$$\eta_{trap} = \sqrt{1 - \left(\frac{n_{air}}{n_{slab}}\right)^2} \simeq 0.74 \qquad (2)$$

which means that almost 26% of photons emitted by the fluorophore leaves the slab within the escape cone and does not reach the lateral sides of the waveguide where the solar cells are placed (Fig. 1(a)). So far, the lost photons have been recycled using different reflectors including diffusive back reflectors, complex mirroring systems using plasmonic structures,[17-21] rugate filters, or opal-like photonic crystals with photonic band gap (PBG) tuned on the emission spectrum.[19, 22-24] More recently, the role of front- and back-reflectors on the performances of LSCs has been modelled[25] and applied to LSCs embedding micro-solar cells into the waveguide.[26]

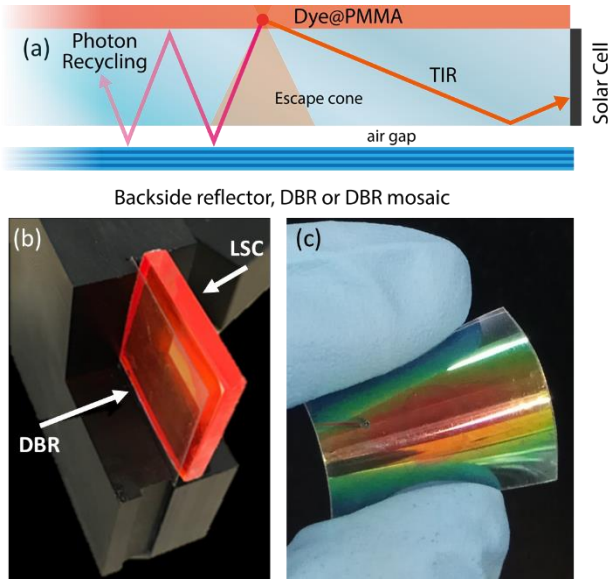

Fig. 1 (a) Schematic of the LSC configuration and main processes involved. Digital photograph of (b) the LSC device coupled to a DBR and (c) of a flexible DBR.

In this work, we report on the role of polymer distributed Bragg reflectors (DBR) as back mirror - in place of a standard diffuser - on the performances of LSCs (Fig. 1(b) and(c)). Polymer DBRs and related structures with very high reflectance in a limited spectral region have been already exploited for lasing, fluorescence emission control, optical switches, and sensors.[27-35] The DBR optical response, including the spectral position of the photonic band-gap, its reflectance intensity and bandwidth, are mainly dictated by the periodicity of the structure and the refractive index contrast among the polymer components.[34] Here, in order to increase the reflection bandwidth, we spun-cast high dielectric contrast polymer DBRs properly tuned to enhance the LSC performances. The DBRs allowed a ~10% enhancement of the optical efficiency that is retained also on scaled-up devices through mosaicking of the DBRs. To this end, we employed both polymers DBRs fabricated alternating commercial cellulose acetate (CA), and poly (*N*-vinyl carbazole) (PVK) layers (sample series P) or CA and the novel processable very high refractive index hydrated titania: poly(vinyl alcohol) nanocomposites (HyTiPVA) (sample series H).

Experimental Section

Fluorophore synthesis and characterization: SilaFluo was synthesized according to literature.[15, 36] Absorption and reflectance spectra were measured at room temperature by an Agilent Cary5000 UV-Vis-NIR spectrophotometer equipped with an Internal Diffuse Reflectance DRA-2500. Fluorescence spectra were measured at room temperature by a Horiba Jobin-Yvon Fluorolog®-3 spectrofluorometer equipped with a 450 W Xenon arc lamp and single and double grating excitation and emission monochromators, respectively.

LSC preparation: To prepare the fluorophore-PMMA layer, about 30 mg of PMMA and SilaFluo were dissolved in ~0.8 mL of chloroform and stirred for 30 min at room temperature. Subsequently, the solution was spread out evenly on thoroughly cleaned 35x50 mm glass surface to obtain a film with thickness 25±5 µm (Starrett micrometer) after evaporation at room temperature in a closed environment. The polymer film was then removed after immersion in water and stored in a desiccator for successive measurements by attaching them on 24x24x3 mm (geometrical factor, G = 8) or 50x50x3 mm (G = 16.7) cleaned glass (Edmund Optics Ltd BOROFLOAT window) with a high-purity silicone oil (poly(methylphenyl siloxane), 710 fluid, Aldrich, n = 1.5365) layer. The diffuser and the DBRs or DBR mosaic (4 DBRs) were placed beneath the LSC with G = 8 (G=16.7).

Preparation of HyTiPVA: the HyTiPVA composite was prepared mixing aqueous solutions of PVA and HyTi with different concentrations adapting a wet synthetic protocol previously reported.[37] HyTi solutions were previously obtained through a controlled hydrolysis of commercial $TiCl_4$ (Sigma-Aldrich, purity>99%) by slow addition of 8 ml of $TiCl_4$ cooled at 0 °C with ice to 62.5 ml of water. The mixtures were maintained under constant stirring at room temperature for 12 h to ensure full reaction. A clear colorless HyTi solution with Ti concentration of 1.03 mmol/L were obtained. To produce the hybrid material, the freshly-prepared HyTi solutions were added to a 20 g/L aqueous solution of PVA (Sigma-Aldrich, ($<M_n>$ = 1.66x10^5 g/mol, 99+% hydrolyzed) at a constant ratio of 1.4:1 v/v. The samples were transparent in the Vis-NIR spectral interval (Fig. S1†), and solution-processable for the preparation of spin-coated films. To this purpose, the filmability of hybrid solutions was optimized by addition of EtOH in the ratio of 1:2 v/v before the mixture deposition.

Polymer DBRs: P series DBR were prepared by spin-coating CA (Aldrich, Mn= 30 000) dissolved in diacetone alcohol (35mg/mL) and PVK (ACROS Organic, Mn=56'400 Mw=135'600) toluene

solutions (28mg/mL) on poly (ethylene terephthalate) (PET) substrates, the rotation speed was kept between 80 and 105 RPS. H series DBR were prepared by casting alternated layers of HyTiPVA and the CA solution on glass substrates with rotation speed ranging between 80 and 120 RPS. More details are reported in Table S1†.

LSC optical efficiency: The optical efficiency of the LSC was measured with a home-built equipment setup. Each DBR, single or mosaic, was placed beneath the LSC of G = 8 or G = 16, respectively. Each sample was tested in triplicate. A solar simulating lamp (ORIEL® LCS-100 solar simulator 94011A S/N: 322, AM1.5G std filter: 69 mW/cm^{-2} at 254 mm) was housed 27.5 cm above the sample. The PV module (IXYS SLMD121H08L mono solar cell 86 x 14 mm) was connected to a digital potentiometer (AD5242) controlled via I2C by an Arduino Uno micro-controller using I2C master library.[38] A digital multimeter (KEITHLEY 2010) was connected in series with the circuit, between the photovoltaic module and the potentiometer, to collect the current as a function of the external load. Conversely, the voltage was measured by connecting the multimeter in parallel to the digital potentiometer.

Optical function characterization: Spectroscopic ellipsometry measurements have been performed on reference thin films of the different materials, by using a VASE instrument by J. A. Woollam Co. in the range (250 – 2500) nm at different angles of incidence from 60° to 75°.[39] Transmittance at normal incidence has been also measured with a Varian Cary 6000i spectrometer in the spectral range (300 – 1800) nm. As a result, the complex refractive index n+ik for all materials was evaluated by WVASE32® software, adopting oscillator models that guarantee for Kramers–Kronig consistency and effective-medium approximation for the HyTiPVA nanocomposite.

Results and discussion

The standard LSC devices were fabricated casting a thin layer of poly(methyl methacrylate) (PMMA) doped with a SilaFluo fluorophore on a glass slab. Then, a diffuser layer was applied to the back of the slab with an air gap (Fig. 1, see Fig. S1† for the optical characterization of the diffuser and of the slab). As mentioned before, the air gap guarantees to maintain the slab guiding properties. This system represents the reference LSC. In our improved LSC devices, the diffuser was replaced with different Bragg stacks maintaining the air gap, as described in the Methods section.

The fluorophore used in this work is a red-emitting 2-amino-7-acceptor-9-silafluorene, where the amino group is –N(CH$_3$)$_2$ the donor, and the acceptor is –CH=C(CN)$_2$ (SilaFluo, Fig. 2(a)). This dye shows fluorescence quantum yield of 65% and has been already successfully used in high performance LSCs.[15, 20] Fig. 2(b) shows the absorbance and fluorescence spectra of the 1.5 wt% SilaFluo embedded in the PMMA film and compares them with the transmittance spectrum normalized to a bare PMMA film. Notwithstanding the absorbance of SilaFluo overlaps the solar emission spectrum only partially, limiting η_{ABS}, it shows a relatively large Stokes shift. Indeed, while the absorption peak is positioned at 478 nm, the fluorescence is centered at 620 nm, limiting re-absorption losses which commonly affect η_{PL}. Moreover, SilaFluo is stable under LSC working conditions and provides an excellent matching with the spectral response of the side Si-solar cells.

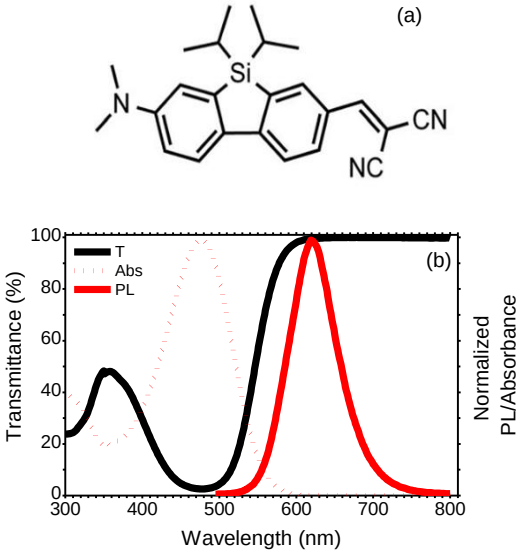

Fig. 2 (a) Silafluo chemical structure. (b) Transmittance and normalized absorbance and photoluminescence spectra of the 1.5 wt.% Silafluo-PMMA film.

Two series of DBRs were fabricated with the CA:PVK and CA:HyTiPVA pairs tuning their PBGs in different spectral regions of the fluorophore emission. Then, the DBRs were placed on the back side of the LSC with the aim to reflect photons leaving the slab from the escape cone (see Fig. 1a). To obtain the best performances from the DBRs, their PBG should be spectrally tuned to the low energy side of the fluorophore emission and should have a large full width at half maximum (FWHM).[25, 26] First, the spectral tuning and the angle of incidence dispersion of the PBG of the DBR allows the mirrors to work finely for all incidence geometry, i.e. for any daily sun illumination conditions.[7, 34, 40] Second, a PBG FWHM larger than the dye fluorescence spectrum is desirable to reflect all the light escaping from the slab. Both the PBG spectral tuning and width are mainly dictated by the periodicity and the dielectric contrast among the DBR components.[34] In a more detail, the PBG position is commonly controlled engineering the layer thicknesses, while its spectral width is only dictated by the dielectric contrast of the materials used. Large dielectric contrast inorganic DBR structures usually gather the best performances,[26] while commodity polymers provide reduced dielectric contrast, but allow very light and flexible mirrors, that can be fabricated even on square meter area (Fig. 1(c)).[34, 41-43] To increase the dielectric contrast in polymer structures, several issues mainly due to the constraint of mutual processability have to be tackled.[29, 30] Indeed, developing suitable high index systems is not straightforward, while the use of low refractive

index polymers suitable for solution growth of DBRs is very complex.[33, 37, 44-46] Only two strategies, which show relevant drawbacks, have been reported so far. For instance, highly porous polymers have very low refractive index,[47, 48] but their high void volume fraction prevents their use for the fabrication of DBR due to percolation of the high index counterpart within the porosity. Low refractive index perfluorinated polymers have been instead successfully employed to spun-cast DBRs,[33, 45] but the cost of such materials is very high and their processability requires specific know-how to allow fine spectral tuning and surface wettability. For these reasons, we decided to use CA as the low refractive index material for DBR fabrication, in fact it is widely employed and easily processable.[34] The refractive index of CA is about 1.47 over a broad spectral region (black line in Fig. 3(a)). In this range, the polymer thin film does not show absorption bands assigned to electronic transitions, which makes it well suitable as transparent material for DBR fabrication. In DBR series P we coupled CA to PVK, which shows instead relevant absorption below 300 nm and a refractive index value of about 1.67 (green line in Fig. 3(a)). Indeed, CA and PVK have been often coupled in literature for the fabrication of polymer DBR for different applications.[34] PVK is currently the solution-processable polymer with the largest refractive index over a very broad spectral range available commercially.[49-52] However, coupling CA and PVK does not allow to achieve dielectric contrast larger than 0.21, thus limiting the PBG width. Moreover, a very large number of periods is necessary to gather reflectance values close to unity.[30, 34, 44]

One of the most promising strategies to achieve large refractive index in polymer matrices consists in the loading of high refractive index nanofillers such at titania nanoparticles (n=2.5).[53] To strongly increase the complex refractive index ($\tilde{n}$) in nanocomposites suitable for photonics two requirements are mandatory. First, large nanofiller volume fractions are needed. Second, a very small size of nanoparticles and no tendency to aggregation are necessary to prevent light scattering and maintain the device transparency. The combination of these requirements, joined to the need of high solution processability, makes this approach challenging.[54] We developed a new processable material with refractive index above the one of PVK. To this end, we refined a method previously reported to strongly increase the refractive index of PVA grafting hydrated titania directly to the hydroxylic group of the polymer.[37, 55] PVA is indeed particularly appealing owing to the large amount of hydroxylic substituents, which can be used as grafting sites for the nanofiller, thus acting as spacers, drastically reducing the aggregation processes and eliminating the need of surfactants (see Methods Section).[56, 57] We then use the new HyTiPVA and CA to spin-cast a series (H) of high performance DBRs with PBG easily tunable on the emission spectrum of the LSC fluorophore. The optical response of the new HyTiPVA material has been determined by spectroscopic ellipsometry and the real part (n) of the complex refractive index ($\tilde{n}$=n+ik) is shown in Fig. 3(a) and compared with other polymers used in this work. The loading results in a dramatic increase of the PVA refractive index. Indeed, while bare PVA shows a refractive index of about 1.55 in the analyzed spectral range (red dashed line in Fig. 3(a)), after the loading the HyTi, the index approaches 1.9 over the entire near infrared and visible spectral regions (red line in Fig. 3(a)). The full spectral response of $\tilde{n}$ is shown in Fig. S2†. From the spectrum reported in Fig. 3(a), according to a simple Maxwell-Garnett effective medium model[53] and considering the refractive index of the HyTiPVA equal to the one of anatase TiO_2, we estimated a volume fraction load of at least 30%. Moreover, no absorption due to electronic transition is detected in the sample spectral range (see also Fig. S2†). These characteristics, together with the good processability of PVA, make the new composite a promising high refractive index medium to be coupled with CA.

The high refractive index of the HyTiPVA hybrid has a remarkable effect on the PBG FWHM. Fig. 3(b) and (c) compare the reflectance spectra of two DBRs made of CA and the high refractive index polymers (HyTiPVA, sample H1 in panel b; PVK, sample P1 in panel c). The reflectance spectra of the sample H1 measured in nine different spots of the sample surface show a large reflectance peak centered at 750 nm with a FWHM of 170 nm, followed by a second order peak centered at 377 nm (Fig. 3(b), more spectral information and photographs are shown in Fig. S3†). Due to the deposition process, the central spot of the sample surface (spot N. 5) commonly differs from the others, affecting the surface homogeneity.[27, 58] On the other hand, the nice overlap of the other spectra, together with the interference pattern testifies the homogeneity and the good optical quality of the sample. The presence of the second order PBG indicates that the mirrors do not fulfill the lambda fourth condition often used for laser cavities,[34] thus possibly allowing wider FWHM. The background provides and average reflectance of about 10%. Comparing the reflectance spectra of the H1 DBR to the LSC emission and transmittance (Fig. 2(b), the emission spectrum is also highlighted in orange in Fig. 3(b) and (c)), we notice the tuning of the first order PBG in the emission spectral region and to its low energy side. DBRs with PBG tuned in different regions have also been fabricated and tested as reported in Fig. S4† for samples H2-H8.

The CA:PVK DBR is instead characterized by a first order PBG at 660 nm with FWHM of 70 nm, positioned on the low energy side of the fluorophore emission (Fig. 3(c)). The second order PBG in this case have a very low intensity and is slightly visible only in two over nine spot measured, demonstrating that the sample is matching the lambda fourth condition.[34] More spectral info and images of this sample are reported in Fig. S5. Comparing the spectra of Fig. 3(b) 3(c) we notice that the CA:PVK sample is less homogeneous than the one fabricated using the HyTiPVA nanocomposite. Moreover, the PBG intensity and width are smaller than for the CA:HyTiPVA DBR but, as shown in the following, this sample provides the best performances when applied to the LSC. Fig. S6† displays the optical characterization of the other samples of the series (P2-P8).

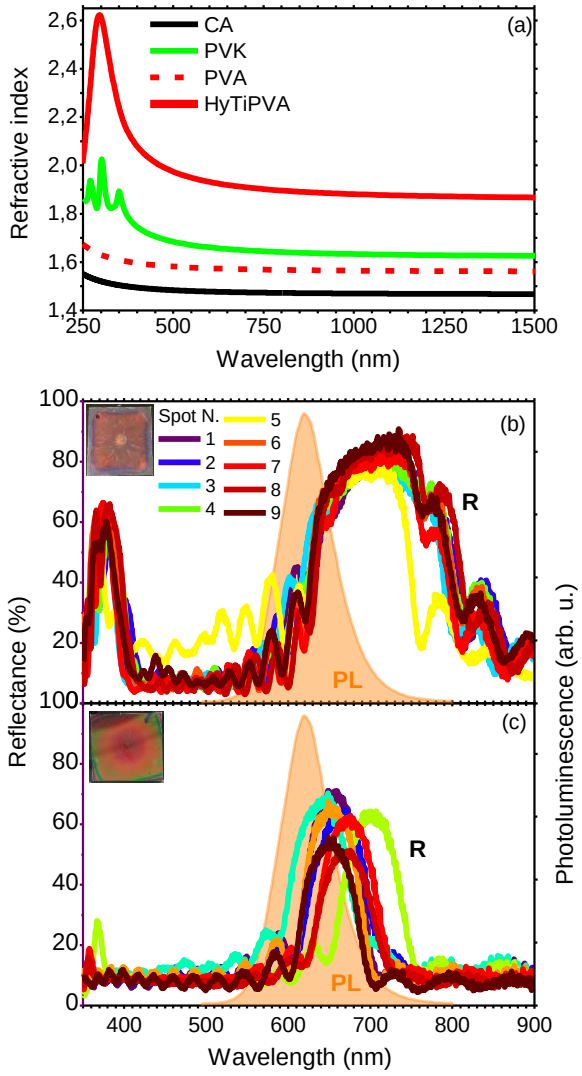

Fig. 3 (a) Refractive index of CA (black line), PVK (green line) from literature,[39, 49, 50] PVA (red dashed line) and HyTiPVA (red continuous line) as retrieved from ellipsometry measurements. (b, c) Reflectance spectra over nine different positions of the polymer DBRs made by CA-HyTiPVA and CA-PVK, respectively. In the same panels, the photoluminescence spectrum of SilaFluo is shown as dashed orange area, while the insets show the digital photographs of the samples.

For what concerns the performances of the SilaFluo-LSCs, we will first focus on devices with size 24x24x3 mm^3. These LSCs have a geometrical factor, that is the ratio between the illuminated surface area and the solar cell area, of G=8. As described before, a diffuser layer is mounted on the back of the reference LSC with an air gap to prevent propagation losses (constant η_{WG}). To assess the DBR effect on the LSC performances we used optical efficiency (η_{opt}^{LSC}) of the side cells integrated spectrally: [59, 60]

$$\eta_{opt}^{LSC} = \frac{C}{G} \qquad (3)$$

where C is the concentration factor, that is the ratio between the maximum current of the PV cell attached the LSC edges under standard solar simulator illumination and the maximum current of the bare cell placed perpendicularly to the lamp (see Experimental Section and Fig. S7 and S8† for details). [59, 60]

For the reference LSC, we found an optical efficiency of 9.4% (Fig. 4) with C=0.75, in full agreement with our recent findings.[15] We then replaced the diffusing layer with CA-HyTiPVA (samples H). The new systems show optical efficiencies ranging from 9.4% to 10.3% with mean 9.7% and standard deviation σ=0.4%, that is up to a 10% enhancement factor. When the diffuser is replaced with the P series of DBRs (CA-PVK), the devices optical efficiency retrieved is more heterogeneous and ranges from 9.3%, which is lower than the reference efficiency, to 10.6%, which represent the best enhancement achieved, the mean value achieved being 9.7% with σ=0.5%.

The larger homogeneity of the data obtained for the H series, can be explained by considering the PBG reflectance intensity and FWHM of the two systems. For the H series, the larger dielectric contrast with respect to the samples prepared with PVK allows wider PBGs, and in turn their overlapping to the largest part of the fluorophore emission spectrum, even for different PBG tuning, making the H series very efficient reflectors for photons leaving the slab within the escape cone (Fig. 1). Then, notwithstanding possible tuning errors and small PBG reflectance value of some of the samples at the PBG (See for instance sample H7 in Fig. S4†), all the samples prepared with the HyTiPVA composite perform better than the reference one with the diffuser. In particular, those samples tuned on the low energy side of fluorophore fluorescence and with large FWHM (H1, H6, H8) provide the best enhancements of optical efficiency due to photon recycling of light for angle of incidence far from the normal direction. Conversely, for CA:PVK DBRs of the series P, both the PBG reflectance intensity and FWHM are relatively small. This characteristic makes the efficiency of the photon recycling more sensitive to the spectral tuning of the photonic structure. These results demonstrate that either a high dielectric contrast or a fine tuning of the photonic structure is necessary to achieve a significant enhancement of the LSC optical efficiency using spun-cast polymer DBRs. We would like to stress that polymer DBRs shows a substantial advantage over standard mirrors used for LSC. Indeed these structures are much lighter and are easily adaptable to any surface (even curved if requested, Fig. 1(c)), and can be eventually grown by different techniques, coextrusion, over square meters at industrial level.[34, 41, 42, 61]

To evaluate the scale-up opportunities of our approach, we also tested the DBRs in mosaic configuration on larger LSC, e.g. by doubling LSC size (G=16). In this case, we created a DBR mosaic coupling the larger LSC to 4 DBR mirrors. Fig. 4(b) shows that for the larger device when the diffuser is used the device optical efficiency does not differ from the previous case. We then exchanged the diffuser with the four-best performing DBRs for each of the two series thus enhancing the efficiency to 10.2% and 10.3% for the H and P series, respectively. Such enhancement, which corresponds to a ~9.5% increase is impressive considering the detrimental effects of the photonic

structure edges, which are known to reduce the LSC performances.[7] Again, the use of industrial techniques previously highlighted for large area DBR production could be of great help to scale-up the dimension of LSC, thus making them a widespread and successful technology.

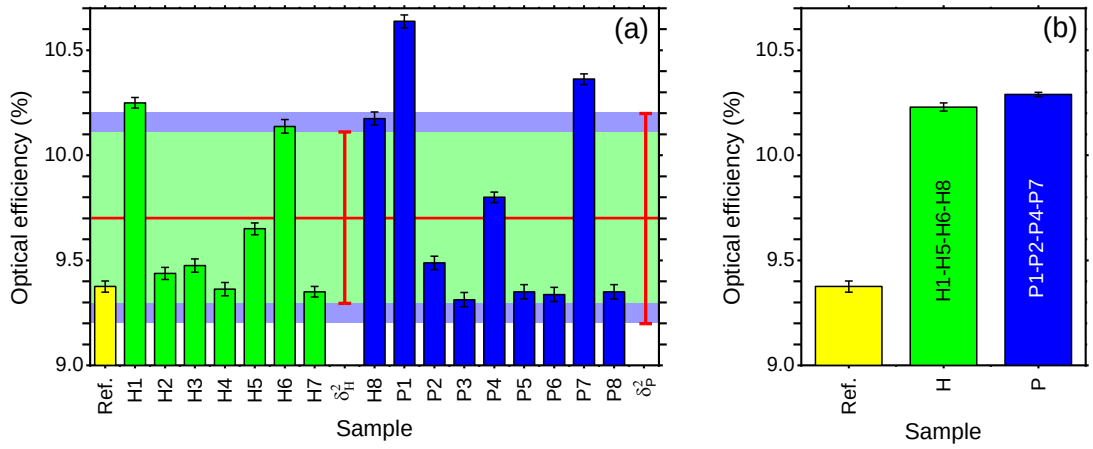

Fig. 4 (a) LSC optical efficiency: reference LSC (yellow bars); LSC with applied DBR of the H (green bars) and P series (blue bars). (b) Optical efficiency for LSC with mosaic DBR mirror. The vertical bars show σ for the two series of DBRs.

Conclusions

We demonstrated that polymer DBRs made of commercial polymers including CA as low index medium and PVK or HyTiPVA nanocomposite fabricated *ad-hoc* by simple wet chemistry can enhance LSCs optical efficiency up to a ~10% increase when used as back reflectors with respect to the same system with a standard diffuser. Moreover, we proved that the enhancement is retained scaling-up of the device area by a factor 4 and using the DBR back reflectors in mosaic configuration. The transparency in the largest part of the visible spectral range of the LSC-DBR devices, together with the possibility to fabricate these systems on the square meter area using industrial techniques pave the way to their application in integrated photovoltaic systems for zero energy consumption buildings in the near future.

Author Contributions

The project was conceived by D.C. and A.P.. G.I. and R.F. fabricated the LSC devices and characterized their performances, P.L., S.S., A. S., G.P. fabricated and characterized the DBR structures, M.P. performed the ellipsometric measurements. M.S. synthetized the SilaFluo dye. Work in Genova was supervised by D.C. and M.A., A.P supervised the work in Pisa. The manuscript was written through contributions of all authors. All authors have given approval to the final version of the manuscript.

Conflicts of interest

There are no conflicts to declare.

Acknowledgements

Work in Genova is supported by the European Union's Horizon 2020 research and innovation program under the Marie Sklodowska-Curie Grant Agreement No. 643238. The authors also acknowledge support from the Universities of Genova and Pisa.

The research leading to these results has received funding from the Università di Pisa under PRA 2017 (project No. 2017_28) and BIHO 2017.

Notes and references

1. V. Balzani and N. Armaroli, *Energy for a sustainable world*, Wiley-VCH, Weinheim, 2010.
2. M. G. Debije and P. P. C. Verbunt, *Adv. Energy Mater.*, 2012, **2**, 12-35.
3. G. Galloro, https://www.eniday.com/it/technology_it/eni-ray-plus-finestre-intelligenti/ https://www.eniday.com/it/technology_it/eni-ray-plus-finestre-intelligenti/, (accessed 14/10/2018).
4. F. Meinardi, H. McDaniel, F. Carulli, A. Colombo, K. A. Velizhanin, N. S. Makarov, R. Simonutti, V. I. Klimov and S. Brovelli, *Nat. Nanotechnol.*, 2015, **10**, 878.
5. P. Moraitis, R. E. I. Schropp and W. G. J. H. M. van Sark, *Opt. Mater.*, 2018, **84**, 636-645.
6. F. Meinardi, F. Bruni and S. Brovelli, *Nat. Rev. Mater.*, 2017, **2**, 17072.
7. A. Bozzola, V. Robbiano, K. Sparnacci, G. Aprile, L. Boarino, A. Proto, R. Fusco, M. Laus, L. C. Andreani and D. Comoretto, *Adv. Opt. Mater.*, 2016, **4**, 147-155.
8. 27 January 2015.
9. F. Meinardi, A. Colombo, K. A. Velizhanin, R. Simonutti, M. Lorenzon, L. Beverina, R. Viswanatha, V. I. Klimov and S. Brovelli, *Nature Photon.* , 2014, **8**, 392-399.

10. I. Coropceanu and M. G. Bawendi, *Nano Lett.*, 2014, **14**, 4097-4101.
11. J. Mei, N. L. C. Leung, R. T. K. Kwok, J. W. Y. Lam and B. Z. Tang, *Chem. Rev.*, 2015, **115**, 11718-11940.
12. A. Pucci, *Isr. J. Chem.*, 2018, **58**, 837-844.
13. R. Mori, G. Iasilli, M. Lessi, A. B. Munoz-Garcia, M. Pavone, F. Bellina and A. Pucci, *Polym. Chem.*, 2018, **9**, 1168-1177.
14. D. Nisi, R. Francischello, A. Battisti, A. Panniello, E. Fanizza, M. Striccoli, X. Gu, N. L. C. Leung, B. Z. Tang and A. Pucci, *Mater. Chem. Front.*, 2017, **1**, 1406-1412.
15. F. Gianfaldoni, F. D. Nisi, G. Iasilli, A. Panniello, E. Fanizza, M. Striccoli, D. Ryuse, M. Shimizu, T. Biver and A. Pucci, *RSC Advances*, 2017, **7**, 37302-37309.
16. J. Yin, D. B. Migas, M. Panahandeh-Fard, S. Chen, Z. Wang, P. Lova and C. Soci, *J. Phys. Chem. Lett.*, 2013, **4**, 3303-3309.
17. F. Mateen, H. Oh, W. Jung, M. Binns and S.-K. Hong, *Sol. Energy*, 2017, **155**, 934-941.
18. M. G. Debije, J.-P. Teunissen, M. J. Kastelijn, P. P. C. Verbunt and C. W. M. Bastiaansen, *Sol. Energy Mater. Sol. Cells*, 2009, **93**, 1345-1350.
19. J. C. Goldschmidt, M. Peters, A. Bösch, H. Helmers, F. Dimroth, S. W. Glunz and G. Willeke, *Sol. Energy Mater. Sol. Cells*, 2009, **93**, 176-182.
20. M. Carlotti, G. Ruggeri, F. Bellina and A. Pucci, *J. Lumin.*, 2016, **171**, 215-220.
21. P. Minei, E. Fanizza, A. M. Rodriguez, A. B. Munoz-Garcia, P. Cimino, M. Pavone and A. Pucci, *RSC Advances*, 2016, **6**, 17474-17482.
22. J. C. Goldschmidt and S. Fischer, *Adv. Opt. Mater.*, 2015, **3**, 510-535.
23. J. Gutmann, J. Posdziech, M. Peters, L. Steidl, R. Zentel, H. Zappe and J. C. Goldschmidt, 2012.
24. A.-L. Joudrier, F. Proise, R. Grapin, J.-L. Pelouard and J.-F. Guillemoles, *Energy Procedia*, 2014, **60**, 173-180.
25. C. Ryan, P. Christian and E. F. Vivian, *J. Opt.*, 2018, **20**, 024009-024001 024009-024013.
26. L. Xu, Y. Yao, N. D. Bronstein, L. Li, A. P. Alivisatos and R. G. Nuzzo, *ACS Photonics*, 2016, **3**, 278-285.
27. P. Lova, G. Manfredi, L. Boarino, A. Comite, M. Laus, M. Patrini, F. Marabelli, C. Soci and D. Comoretto, *ACS Photonics*, 2015, **2**, 537-543.
28. P. Lova, C. Bastianini, P. Giusto, M. Patrini, P. Rizzo, G. Guerra, M. Iodice, C. Soci and D. Comoretto, *ACS Appl. Mater. Interfaces*, 2016, **8**, 31941–31950.
29. P. Lova, V. Grande, G. Manfredi, M. Patrini, S. Herbst, F. Würthner and D. Comoretto, *Adv. Opt. Mater.*, 2017, **5**, 1700523.
30. G. Manfredi, P. Lova, F. Di Stasio, R. Krahne and D. Comoretto, *ACS Photonics*, 2017, **4**, 1761–1769.
31. P. Lova, D. Cortecchia, H. N. S. Krishnamoorthy, P. Giusto, C. Bastianini, A. Bruno, D. Comoretto and C. Soci, *ACS Photonics*, 2018, **5**, 867-874.
32. G. Manfredi, P. Lova, F. D. Stasio, P. Rastogi, R. Krahne and D. Comoretto, *RSC Advances*, 2018, **8**, 13026.
33. P. Giusto, P. Lova, G. Manfredi, S. Gazzo, P. Srinivasan, S. Radice and D. Comoretto, *ACS Omega*, 2018, **3**, 7517-7522.
34. P. Lova, G. Manfredi and D. Comoretto, *Adv. Opt. Mater.*, 2018, DOI: doi:10.1002/adom.201800730.
35. P. Lova, *Polymers*, 2018, **10**, 1161.
36. M. Shimizu, K. Mochida, M. Katoh and T. Hiyama, *J. Phys. Chem. C*, 2010, **114**, 10004-10014.
37. M. Russo, M. Campoy-Quiles, P. Lacharmoise, T. A. M. Ferenczi, M. Garriga, W. R. Caseri and N. Stingelin, *J. Polym. Sci., Part B: Polym. Phys.*, 2012, **50**, 65-74.
38. Arduino, https://www.arduino.cc, (accessed 10/10/2018).
39. *WVASE32® software; b. J. A. Woollam Co., Inc.*
40. D. Comoretto, ed., *Organic and Hybrid Photonic Crystals*, Springer International Publishing, Cham, 2015.
41. T. Kazmierczak, H. Song, A. Hiltner and E. Baer, *Macromol. Rapid Commun.*, 2007, **28**, 2210-2216.
42. H. Song, K. Singer, J. Lott, Y. Wu, J. Zhou, J. Andrews, E. Baer, A. Hiltner and C. Weder, *J. Mater. Chem.*, 2009, **19**, 7520-7524.
43. Chamleonlab, https://www.chameleonlab.nl/, http://chameleonlab.nl/, (accessed 14/10/2018).
44. S. Gazzo, G. Manfredi, R. Poetzsch, Q. Wei, M. Alloisio, B. Voit and D. Comoretto, *J. Polym. Sci., Part B: Polym. Phys.*, 2016, **54**, 73-80.
45. 2016.
46. T. S. Kleine, L. R. Diaz, K. M. Konopka, L. E. Anderson, N. G. Pavlopolous, N. P. Lyons, E. T. Kim, Y. Kim, R. S. Glass, K. Char, R. A. Norwood and J. Pyun, *ACS Macro Lett.*, 2018, **7**, 875-880.
47. W. Gaëtan, F. Rolando, S. Stefan and Z. Libero, *Macromol. Chem. Phys.*, 2010, **295**, 628-636.
48. J. Q. Xi, M. F. Schubert, J. K. Kim, E. F. Schubert, M. Chen, S.-Y. Lin, W. Liu and J. A. Smart, *Nature Photon.*, 2007, **1**, 176-179.
49. L. Frezza, M. Patrini, M. Liscidini and D. Comoretto, *J. Phys. Chem. C*, 2011, **115**, 19939-19946.
50. L. Fornasari, F. Floris, M. Patrini, D. Comoretto and F. Marabelli, *Phys. Chem. Chem. Phys.* , 2016, **18**, 14086-14093.
51. L. Moroni, P. R. Salvi, C. Gellini, G. Dellepiane, D. Comoretto and C. Cuniberti, *J. Phys. Chem. A*, 2001, **105**, 7759-7764.
52. D. Comoretto, C. Cuniberti, G. F. Musso, G. Dellepiane, F. Speroni, C. Botta and S. Luzzati, *Phys. Rev. B*, 1994, **49**, 8059-8066.
53. R. J. Gher and R. W. Boyd, *Chem. Mater.*, 1996, **8**, 1807–1819.
54. J.-g. Liu and M. Ueda, *J. Mater. Chem.*, 2009, **19**, 8907–8919.
55. M. Russo, S. E. J. Rigby, W. Caseri and N. Stingelin, *J. Mater. Chem.*, 2010, **20**, 1348-1356.
56. T. Yovcheva, I. Vlaeva, I. Bodurov, V. Dragostinova and S. Sainov, *Appl. Opt.*, 2012, **51**, 7771-7775.
57. S. Mahendia, A. Kumar Tomar, P. K. Goyal and S. Kumar, *J. Appl. Phys.*, 2013, **113**, 073103.
58. G. Manfredi, C. Mayrhofer, G. Kothleitner, R. Schennach and D. Comoretto, *Cellulose*, 2016, **23**, 2853-2862.
59. Z. Krumer, W. G. J. H. M. van Sark, R. E. I. Schropp and C. de Mello Donegá, *Sol. Energy Mater. Sol. Cells*, 2017, **167**, 133-139.
60. Y. Zhao and R. R. Lunt, *Adv. Energy Mater.*, 2013, **3**, 1143-1148.
61. TORAY, https://www.toray.com/, http://www.toray.com, (accessed 14/10/2018).